Segmentation of Palm Vein Images Using U-Net

Felix Marattukalam and Waleed H. Abdulla
The University of Auckland, New Zealand
E-mail: (felix.marattukalam,w.abdulla)@auckland.ac.nz

***Abstract*—Biometric recognition methods using human traits like fingerprint, face, voice, palm-print, and palm vein have developed significantly in recent years. Palm vein recognition has gained attention because of its unique characteristics and high recognition accuracy. Many palm vein recognition methods proposed recently suffer from the issue of having low-quality images right at the acquisition stage, resulting in degradation of recognition accuracy. This paper proposes the use of a Convolutional Neural Network (CNN); U-Net, to effectively segment the vein networks from the background of near-infrared palm vein images. The experiments were conducted on the HK PolyU Multispectral Palmprint and Palmvein database. The original images taken from the database were reduced to region of interests. Morphological operations were applied to obtain ground truth mask images. The mask images were then used to train a modified U-Net in which Gabor filter was applied in the first block of the U-Net architecture. The accuracy of the segmented vein images was obtained by determining the overlap between the segmented images obtained from the network and the corresponding ground truth images from the morphological operations. The overlap is evaluated using the Jaccard Index and Dice Coefficient Metrics. For both of these similarity metrics, the value "0" indicates no overlap and "1" indicates a complete congruence between the subject images. The best Dice Coefficient obtained in this experiment is 0.69 and the Jaccard Index is 0.71, which makes this technique promising for automatic vein segmentation and can be adopted in palm vein recognition systems.**

I. Introduction

Palm vein recognition has been a topic of interest for researchers in recent years. It is a biometric recognition method in which the palm vein patterns are used as features for authentication (one-to-one user comparison) or identification (one-to-N user comparison). Vein patterns, which are unique [1], [2], can be made visible under Near-Infrared Light (NIR) [3], [4]. NIR light having wavelengths in the range of 760 nm – 820 nm penetrates the skin to a depth of 5mm [5], [6]. Veins carrying deoxygenated blood absorb the NIR light, whereas the skin and surrounding tissues reflect it [5]. Due to this attribute, the veins appear as a dark network. This network is then captured using an infrared-sensitive camera. Once the images are captured, they are pre-processed to extract suitable features that can be used by the recognition system. Feature extraction primarily consists of vein network segmentation from the background information. This segmentation has remained a challenging topic affecting the recognition systems. The information that is obtained from the segmented images can be used to generate ground truth feature maps. These feature maps can further be used as templates to train neural networks for the recognition process. An automated solution to segment the palm vein images would improve the recognition accuracy of palm vein biometric systems significantly. Since 2012, Convolutional Neural Networks (CNNs) have widely been applied for image classification and semantic segmentation problems in biometrics. CNN architectures like AlexNet, GoogLeNet, and VGGNet are being used to obtain global class probability per image and have proven to be extremely efficient and accurate in this field [7]. The problem of semantic segmentation in palm vein is somewhat more complex as the number of output probabilities is directly proportional to the number of pixels in an image. Fully Convolutional network (FCN) introduced by Long et.al [8] was able to train end-to-end with the image information shared between the up-sampling and down-sampling paths thus improving the segmentation. U-Net [9], unlike FCN is different in the decoder path. FCN uses skip connections to enhance the segmentation whereas, U-Net uses it to enhance the up-sampled features in the decoder part of the network. U-Net also handles the data scarcity problem in the biometric and biomedical domain. Unlike normal CNNs, U-Net consists of encoder layers and decoder layers. Encoder layer reduces the spatial dimensions of the image, whereas decoder layer gradually repairs the details in the spatial dimension of the image. The encoder and decoder layers are interconnected so that the decoder layer can repair and recreate the target details. The final layer consists of the probability of each pixel belonging to the respective classes which, in this case, would be either, the vein or the skin.

In this paper, we propose a new palm vein segmentation technique using the Convolutional Neural Network U-Net to segment the vein network. The encoder layer of the U-Net architecture is modified with a custom Gabor Filter to extract the vein features. The experiments were performed on HK PolyU Multispectral Palm vein and Palm-print database [10]. The obtained results are promising when compared to the commonly adopted palm vein segmentation methods.

This paper is organized as follows. Section II discusses a few promising recent palm vein segmentation methods based on traditional approaches and deep neural networks. In section III, the proposed algorithm is presented. Section IV reports the obtained experimental results, while section V concludes this paper highlighting the performance of the proposed technique in vein biometric segmentation.

II. Vein Segmentation in Biometric

Vein segmentation for ground truth template generation can be done using multiple techniques. The two preferred methods are where the biometric features transformed into quantized feature vectors and where the original features retained without any transformation. The quantized feature transformation aims at reducing the computational complexity and employs more traditional comparison methods for recognition. Whereas when the features are retained, the matching process is computationally intensive but has higher recognition accuracy.

In [11], the palm vein features are extracted by using an optimized algorithm using 2D Gabor filter. The feature vectors are encoded and good recognition performance is achieved using simple templates. However, the template security is not analyzed. In [12], 2D Gabor filter has been used in a directional coding technique. Its performance does not estimate the optimum parameters of Gabor filter. In [13], 2D palm hash code is constructed using both, palmprint and palm vein. They used a Gabor filter for feature extraction. Scale Invariant Feature Transform (SIFT) is often used in palm vein systems.In [14], SIFT matching is used for palm vein verification. The feature points are represented by SIFT descriptors. Each descriptor is a 128 dimension vector and the total size of the template depends on the number of descriptors that have been detected. In [15], Local Invariant features from multiple samples are extracted using SIFT. [16] uses root SIFT which is a variation of SIFT for feature extraction and matching. It is a more stable feature extraction technique. Root SIFT and SIFT schemes are computationally expensive as the template features have to be retained.In [17], two methods are proposed i.e. Hessian matrix based and Radon transform based for identification. The Hessian matrix method extracts the features using the eigen values of the Hessian matrix. This method offers good recognition performance with small size ground truth template, hence being computationally efficient. Methods in which palm vein images are retained by just enhancing the images and used in the biometric systems are computationally inefficient because of large template size resulting in longer processing speeds during the matching process. In [18], an improved Local Binary pattern based scheme is used. This method achieves high verification accuracy. However, the templates' efficiency with respect to privacy and size is not reported. In [19], wavelet transform has been used for local feature extraction which does not provide high recognition accuracy. In [20], wave atom transform based palm vein recognition scheme is proposed. The scheme maintains and matches the palm vein templates with less computational complexity and large storage requirements.

Many works based on Gabor filters [11], [13], match filters [21], wide line detectors [22], and neural networks are proposed for vein based verification systems. The assumptions made in these systems suffer the following few problems [23]. a) It is not always effective to extract the vein patterns, b) it is impossible to describe the attributes of all distributions created by the pixels, c) it is difficult to develop a mathematical model to effectively model the distributions. Deep learning methods are more effective and hence more robust for both, ground truth template generation

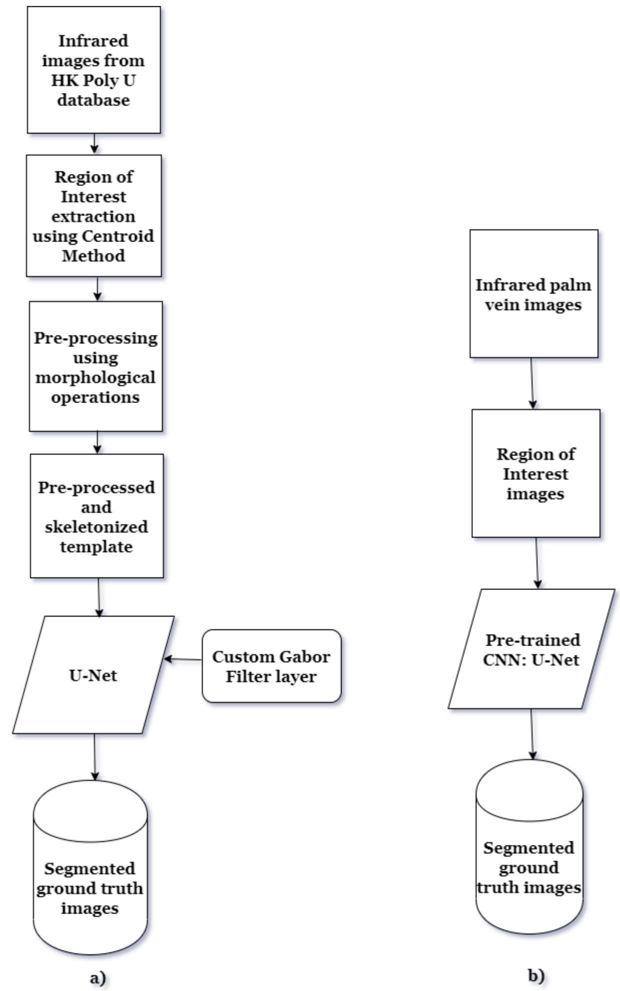

Fig. 1: Flowchart of the proposed system a) Training phase and b) Testing phase

and feature mapping in vein biometric systems. Some researchers brought it into medical segmentation [24], [25] such as retina image segmentation, brain segmentation and neuronal membrane segmentation.Convolutional neural networks have outperformed the state of the art computer vision applications for segmentation [23]. Different from the above mentioned segmentation methods, deep learning segmentation method is an end-to-end architecture without the manual attribute distribution assumption. However, many vein patterns show more complex shape instead of a valley or straight line and hence differing from the assumptions made. Based on the optimal performance of U-Net in the field of medical image segmentation [9], we employ it for palm vein segmentation.

III. The Proposed method

A. Overview of proposed method

The overall flowchart of palm vein segmentation using U-Net proposed in this study is shown in Fig.1.

First, the palm vein infrared images are reduced to the region of interest (ROI) using the centroid method [26]. The obtained ROI images are of the resolution 128 x 128 pixels. The images are enhanced using adaptive thresholding. Morphological operation of iterative erosion followed by dilation are applied on the images to obtain a binary mask with minimum noise. Medial axis thinning algorithm [27] is applied on the resultant images to skeletonize the vein network and obtain the final mask images which are then used to train the U-Net with the custom Gabor filter layer. Once the U-Net is trained, it can automatically segment any palm vein image to generate reliable ground truth images for recognition systems.

B. Region of Interest

This step aims to reduce the palm vein image to a specific region of interest. Often in palm vein recognition systems, the whole palm image is not necessary for recognition. A small region of palm consisting of the unique pattern is sufficient to recognize the user. This also helps in reducing the template size and hence makes the overall system algorithms computationally efficient.

For a two dimensional image which is continuous, $f(x,y)(\geq 0)$, the m_{pq} of $p+q$ moment is given by (1) and the central moment μ_{pq} is given by (2).

$$m_{pq} = \int_{-\infty}^{\infty}\int_{-\infty}^{\infty} x^p y^q f(x,y)dxdy \tag{1}$$

$$\mu_{pq} = \int_{-\infty}^{\infty}\int_{-\infty}^{\infty} (x-\bar{x})^p (y-\bar{y})^q f(x,y)dxdy \tag{2}$$

Where p and q are non-negative integers. For a digital image which is discrete and discontinuous, the formulae can be transformed to be (3) and (4):

$$m_{pq} = \sum_{j=1}^{N}\sum_{i=1}^{N} i^p j^q f(i,j) \tag{3}$$

$$\mu_{pq} = \sum_{j=1}^{N}\sum_{i=1}^{N} (i-i_c)^p (j-j_c)^q f(i,j) \tag{4}$$

The zeroth and first order moments are (5), (6) and (7):

$$m_{00} = \sum_{j=1}^{N}\sum_{i=1}^{N} f(i,j) \tag{5}$$

$$m_{10} = \sum_{j=1}^{N}\sum_{i=1}^{N} if(i,j) \tag{6}$$

$$m_{01} = \sum_{j=1}^{N}\sum_{i=1}^{N} jf(i,j) \tag{7}$$

Here, i_c, j_c are the coordinates of the centroid, which are given by (8) and (9)

$$i_c = \frac{m_{10}}{m_{00}} \tag{8}$$

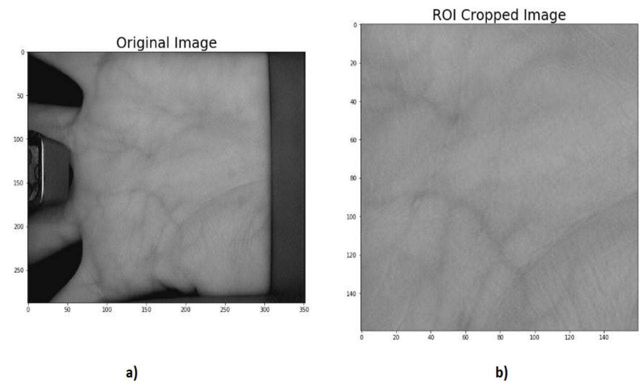

Fig. 2: a) Original image b) ROI extracted from original image using centroid method

$$j_c = \frac{m_{01}}{m_{00}} \tag{9}$$

The procedure can be summarized as follows. Each original image from the database is taken and the above mentioned centroid method applied on it. The obtained result is the ROI image as shown in Fig. 2 with a resolution of 128 x 128 pixels.

C. Morphological operations

Once the region of interest image is obtained, the next major step is to extract the vein features.

Thresholding is applied on this image to manually segment the image by setting all the pixels whose intensity values are above a threshold to a foreground value, in this case, white color for vein and the other pixels to the background value having black color. Unlike conventional thresholding, which uses a global threshold, adaptive thresholding is applied. The local threshold is calculated statistically by examining the intensity values of each neighborhood pixel. Morphological image processing methods are applied on the obtained image.

The binary image obtained contains numerous imperfections. Morphological image processing methods help remove these imperfections. Erosion and dilation are the two fundamental morphological operations. Erosion removes all the small scale details from the binary image affecting the region of interest by reducing it to background information. Dilation does the exact opposite of this by changing both size and shape of the vein networks. Open morphological operation is a compound operation of erosion followed by dilation. Medial axis transform for the skeletonization of the extracted images is then performed. Skeletonization shrinks the foreground region, in this case, veins to skeletal remnants. Fig. 3 gives the result obtained after performing morphological operations and skeletonization on a ROI image.

D. U-Net architecture

The U-Net is different from a conventional Convolutional Neural Network since it consists of encoder and decoder layers. Encoder layers are responsible for the dimensional

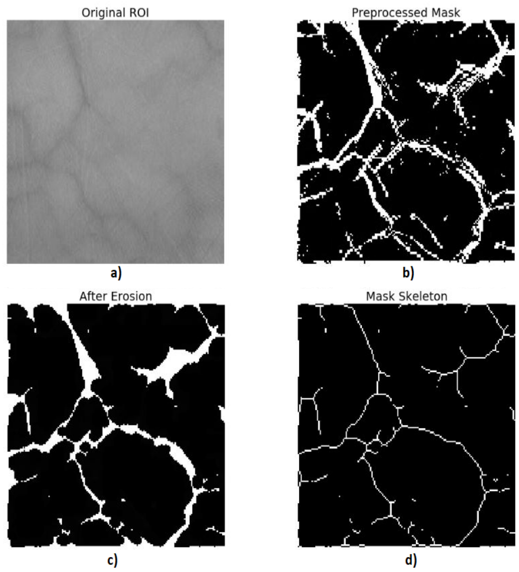

Fig. 3: Feature extraction using morphological method a) Original ROI image b) Pre-processed mask image c) Erosion-dilation operation output d) Skeletonized mask image

reduction of the image while the decoder layers repair the image details. The encoder and decoder layers are connected for information retention within the image, thus helping in better repairing of the target image and hence the name U-Net. The last layer of the network calculates the output probability of each pixel, which belongs either to the palm vein network or the background. The U-Net network architecture used in this experiment is shown in Fig. 4.

The architecture looks like a 'U' as can be seen in Fig.4. This architecture consists of three sections: the contraction, the bottleneck, and the expansion section. The contraction section is made of multiple contraction blocks. Each block takes an input image and applies two 3x3 convolution layers followed by a 2x2 max pooling operation. The number of kernels or feature maps after each block doubles so that the architecture can learn the complex structures in the images effectively. The intermediate layer mediates between the contraction and the expansion section. It uses two 3x3 CNN layers followed by a 2x2 up convolution layer. This structure is then followed by the expansion section. Similar to contraction section, it consists of multiple expansion blocks. Each block passes the input to two 3x3 convolutional neural network layers followed by a 2x2 upsampling layer. Also, after each block, the number of feature maps used by convolutional layer reduces to half to maintain the symmetry. However, every time the input also gets appended by the feature maps of the corresponding contraction layer. This would ensure that the features learned while contracting the image will now be used to reconstruct it. The number of expansion blocks is same as the number of contraction blocks. The resultant mapping passes through another 3x3 CNN layer with the number of feature maps equal to the number of segments desired.

To train the U-Net, 6000 images from the database were used (12 images per class, the total number of classes was 500). 80:20 split of the database was done for training and testing purposes. An adaptive learning algorithm called Adam Optimizer with a learning rate lr = 0.00015 was used. The accuracy and loss function was set as Dice Coefficient for the first training session and Jaccard Index for the second session. The network was trained and evaluated for 20, 30, 40 and 50 epochs respectively. In the first block, a custom Gabor filter was used. A Gabor filter is a sinusoidal signal of a particular frequency which is modulated by a Gaussian wave. The filter has real and imaginary components that represent orthogonal directions. The two components can be used independently or can form a complex number. Equations (10), (11) and (12) show the parameters that control the shape and size of the Gabor filter.

$$g(x,y;\lambda,\theta,\psi,\sigma,\gamma) = \exp\left(-\frac{x'^2+\gamma^2 y'^2}{2\sigma^2}\right)\exp\left(i\left(2\pi\frac{x'}{\lambda}+\psi\right)\right) \tag{10}$$

$$g(x,y;\lambda,\theta,\psi,\sigma,\gamma) = \exp\left(-\frac{x'^2+\gamma^2 y'^2}{2\sigma^2}\right)\cos\left(2\pi\frac{x'}{\lambda}+\psi\right) \tag{11}$$

$$g(x,y;\lambda,\theta,\psi,\sigma,\gamma) = \exp\left(-\frac{x'^2+\gamma^2 y'^2}{2\sigma^2}\right)\sin\left(2\pi\frac{x'}{\lambda}+\psi\right) \tag{12}$$

where

$$x' = x\cos\theta + y\sin\theta \tag{13}$$

$$y' = -x\sin\theta + y\cos\theta \tag{14}$$

Here, λ is the wavelength of the sinusoidal component, θ is the orientation of the normal to the parallel stripes of Gabor function, ψ is the phase offset of the sinusoidal function, σ is the standard deviation of the Gaussian envelope and γ is the spatial aspect ratio which specifies the ellipticity of the Gabor function. K-type indicates the type and range of values that each pixel in a Gabor kernel can hold. Table I shows the Gabor filter parameters used in this experiment.

TABLE I: Values for Gabor Filter used

Kernel Size	σ	θ	γ	ψ
3 x 2	1	1	0.3	π x 0.5

IV. Results and Discussion

A. Qualitative evaluation

We selected one representative sample from the 6000 images on which we performed the experiment. The obtained results are shown in Fig.5. The results visually demonstrate that the proposed segmentation is accurate when it is being compared to the original image superimposed with the manual annotation.

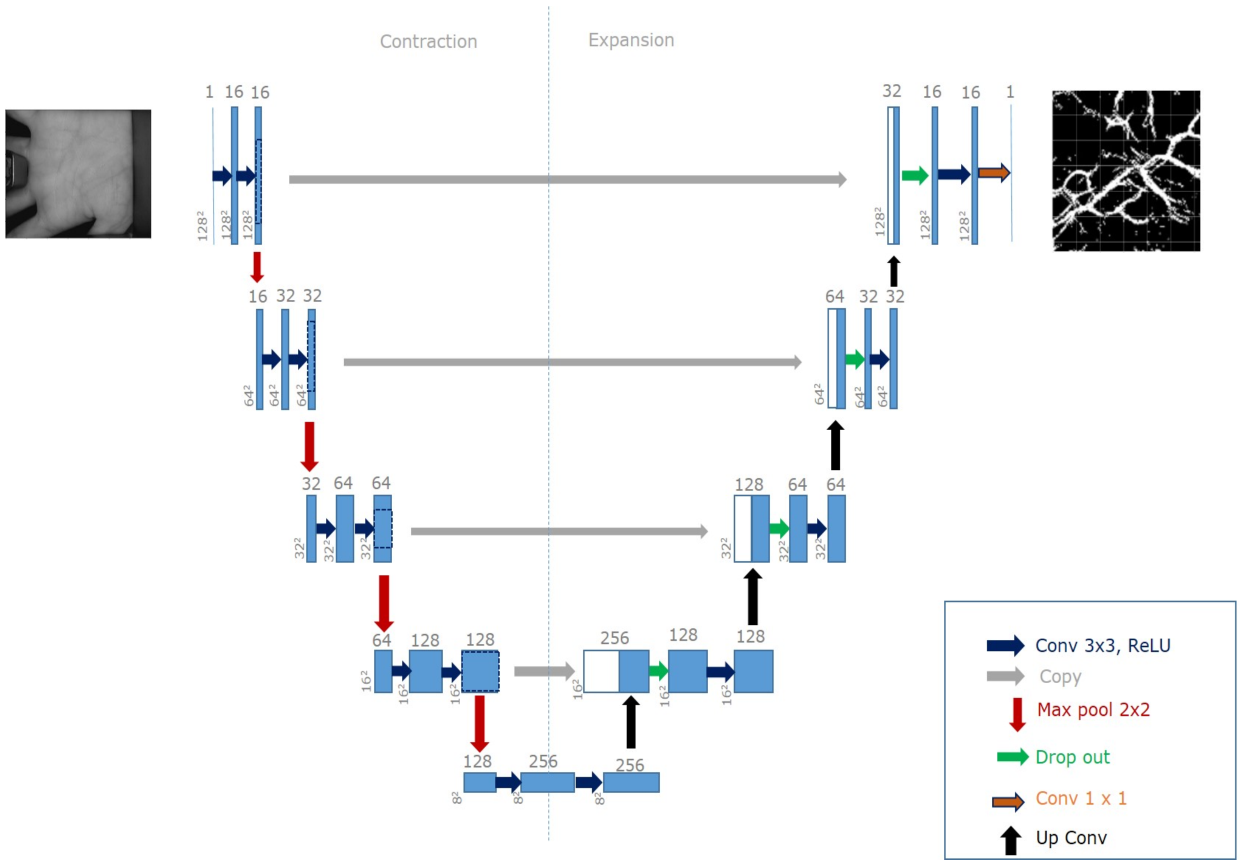

Fig. 4: U-Net network architecture for palm vein segmentation

B. *Quantitative evaluation*

In medical image segmentation problems, manually labeled images by experts for each subject is used as a gold standard. The standard gold image is then compared with the binary image template which the segmentation algorithm provides. However, to the best of our knowledge, there is no database with gold standard manual annotated labels to evaluate this segmentation. Thus, we have evaluated the quantitative performance of the model by computing the similarity accuracy measure and loss function, namely, Dice Coefficient (DC) and the Jaccard Index (J).

1) Dice Coefficient (DC): Dice coefficient measures the extent of spatial overlap between two binary images. Its values range between "0", indicating no overlap, and "1" indicating perfect overlap. The DC value is computed using (15).

$$DC = \frac{2 \mid S \cap M \mid}{\mid S \mid + \mid M \mid} \tag{15}$$

Where the segmentation result is denoted by S, while the manual segmentation or the morphological operation output is denoted by M.

2) Jaccard Index (J): The Jaccard index or Jaccard coefficient is used to measure the spatial overlap of the intersection divided by the union of two labeled sets. It can be expressed by (16). It can also be deduced from Dice Coefficient using (17).

TABLE II: Dice Coefficient And Jaccard Index Values

Type	Dice Coefficient	Jaccard Index
Comparison - 1	0.6975	0.7131
Comparison - 2	0.7245	0.7122

$$J = \frac{\mid S \cap M \mid}{\mid S \cup M \mid} \tag{16}$$

$$J = \frac{DC}{(2 - DC)} \tag{17}$$

These similarity metrics are calculated and compared between the morphological output and the segmented output for the first comparison (Comparison - 1), and between the manually annotated image and segmented output for the second comparison (Comparison - 2). The obtained results are listed in Table II.

Fig. 6 and Fig. 7 show the accuracy and loss metric plots for one of the evaluation session using twenty epochs. In this case, Dice Coefficient is the selected metric for both, accuracy and loss measurements. Accuracy measures the network's performance by counting the number of predictions where the

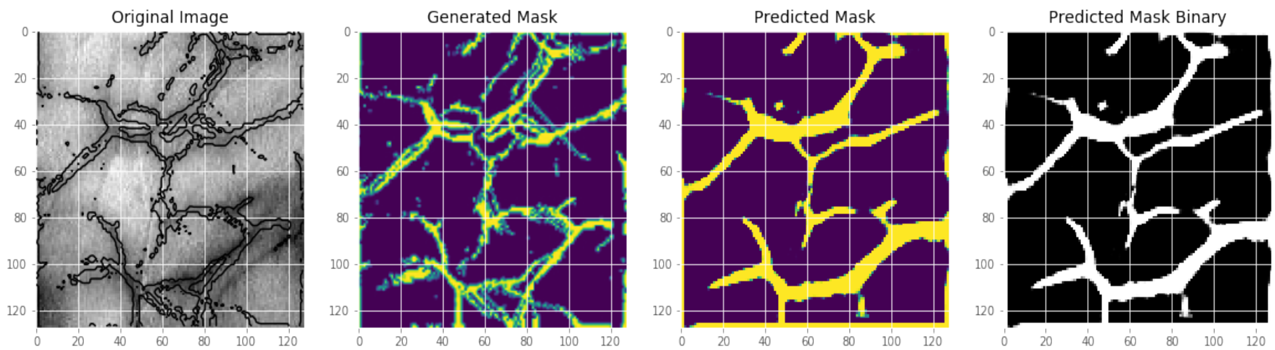

Fig. 5: Segmentation results using the proposed method a) The original ROI image with manual annotation b) Mask generated using the morphological methods c) The mask that was predicted by the proposed method d) Binary image of the final mask which is the segmented output from the proposed method

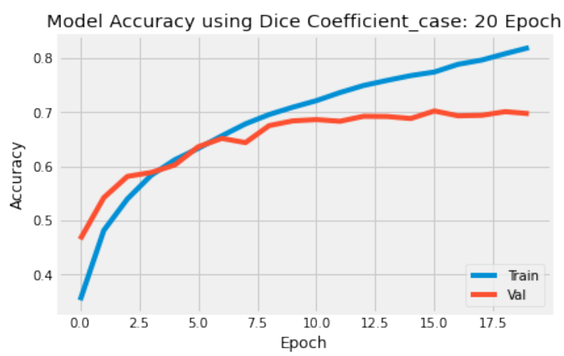

Fig. 6: Comparison 1: Model accuracy using Dice Coefficient

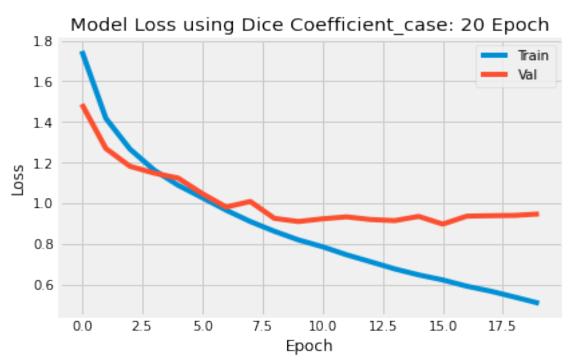

Fig. 7: Comparison 1: Model loss using Dice Coefficient

predicted value is equal to the true value. Here, it measures the similarity between the image predicted using the U-Net model and the output images obtained after the morphological operations. Loss function, also known as cost function, takes into account the uncertainty of a prediction based on the differences observed when compared to the true value. The loss function used during the network training phase was the Dice coefficient loss.

V. Conclusion

This paper presents a new method to segment infrared palm vein images using a modified U-Net architecture. The images taken from the database are reduced to the ROI using Centroid method. Morphological operations are then used on the obtained ROI images to further process them by mainly applying adaptive thresholding and erosion. Medial thinning algorithm is used to shrink the width of the vein network outputs obtained from the morphological operations step to their skeletal form. These images are used to train a U-Net, which has a custom modified Gabor filter layer. The results show that the proposed technique is able to segment the palm vein network with a good accuracy. Since there is no state-of-the-art method proposed to compare our results, we used the standard segmentation similarity metric that is most commonly used in medical segmentation, namely, Dice Coefficient and Jaccard Index. The best Dice Coefficient value for the comparison between the morphological output and segmented results was 0.697 and for the comparison between manually annotated ground truth and segmented image was 0.724. This indicates approximately 70% accuracy of the segmented results making this method promising to generate reliable ground truth images to train neural networks for palm vein recognition systems.

Our future work will be to use these ground truth images in a recognition system and compute the standard recognition evaluation parameters like False Acceptance Rate (FAR), False Rejection Rate (FRR), Equal Error Rate (EER) and Region of Convergence (ROC). This will help design robust palm vein recognition systems.

Acknowledgment

We would like to thank the authors of HK PolyU Multi-spectral Palm-print database for making their database publicly available which has been used in this research experiment.

References

[1] M. Watanabe, “Palm vein authentication,” in *Advances in biometrics*. Springer, 2008, pp. 75–88.

[2] J.-C. Lee, "A novel biometric system based on palm vein image," *Pattern Recognition Letters*, vol. 33, no. 12, pp. 1520–1528, 2012.

[3] T. Shinzaki, "Use case of palm vein authentication," in *Handbook of Vascular Biometrics*. Springer, Cham, 2020, pp. 145–158.

[4] L. Wang and G. Leedham, "Near-and far-infrared imaging for vein pattern biometrics," in *2006 IEEE International Conference on Video and Signal Based Surveillance*. IEEE, 2006, pp. 52–52.

[5] M. Clement, G. Daniel, and M. Trelles, "Optimising the design of a broad-band light source for the treatment of skin," *Journal of Cosmetic and Laser Therapy*, vol. 7, no. 3-4, pp. 177–189, 2005.

[6] F. Marattukalam and W. H. Abdulla, "On palm vein as a contactless identification technology," in *2019 Australian & New Zealand Control Conference (ANZCC)*. IEEE, 2019, pp. 270–275.

[7] A. Garcia-Garcia, S. Orts-Escolano, S. Oprea, V. Villena-Martinez, and J. Garcia-Rodriguez, "A review on deep learning techniques applied to semantic segmentation," *arXiv preprint arXiv:1704.06857*, 2017.

[8] J. Long, E. Shelhamer, and T. Darrell, "Fully convolutional networks for semantic segmentation," in *Proceedings of the IEEE conference on computer vision and pattern recognition*, 2015, pp. 3431–3440.

[9] O. Ronneberger, P. Fischer, and T. Brox, "U-net: Convolutional networks for biomedical image segmentation," in *International Conference on Medical image computing and computer-assisted intervention*. Springer, 2015, pp. 234–241.

[10] H. PolyU. Polyu multispectral palmprint database. [Online]. Available: http://www.comp.polyu.edu.hk/ biometrics/MultispectralPalmprint/MSP.htm

[11] W.-Y. Han and J.-C. Lee, "Palm vein recognition using adaptive gabor filter," *Expert Systems with Applications*, vol. 39, no. 18, pp. 13 225–13 234, 2012.

[12] R. R. Fletcher, V. Raghavan, R. Zha, M. Haverkamp, and P. L. Hibberd, "Development of mobile-based hand vein biometrics for global health patient identification," in *IEEE global humanitarian technology conference (GHTC 2014)*. IEEE, 2014, pp. 541–547.

[13] L. Leng, M. Li, and A. B. J. Teoh, "Conjugate 2dpalmhash code for secure palm-print-vein verification," in *2013 6th International Congress on Image and Signal Processing (CISP)*, vol. 3. IEEE, 2013, pp. 1705–1710.

[14] P.-O. Ladoux, C. Rosenberger, and B. Dorizzi, "Palm vein verification system based on sift matching," in *International Conference on Biometrics*. Springer, 2009, pp. 1290–1298.

[15] X. Yan, W. Kang, F. Deng, and Q. Wu, "Palm vein recognition based on multi-sampling and feature-level fusion," *Neurocomputing*, vol. 151, pp. 798–807, 2015.

[16] W. Kang, Y. Liu, Q. Wu, and X. Yue, "Contact-free palm-vein recognition based on local invariant features," *PloS one*, vol. 9, no. 5, p. e97548, 2014.

[17] Y. Zhou and A. Kumar, "Human identification using palm-vein images," *IEEE transactions on information forensics and security*, vol. 6, no. 4, pp. 1259–1274, 2011.

[18] W. Kang and Q. Wu, "Contactless palm vein recognition using a mutual foreground-based local binary pattern," *IEEE transactions on Information Forensics and Security*, vol. 9, no. 11, pp. 1974–1985, 2014.

[19] J.-G. Wang, W.-Y. Yau, A. Suwandy, and E. Sung, "Person recognition by fusing palmprint and palm vein images based on "laplacianpalm" representation," *Pattern recognition*, vol. 41, no. 5, pp. 1514–1527, 2008.

[20] F. Ahmad, L.-M. Cheng, and A. Khan, "Lightweight and privacy-preserving template generation for palm-vein-based human recognition," *IEEE Transactions on Information Forensics and Security*, vol. 15, pp. 184–194, 2019.

[21] Z. Zhang, S. Ma, and X. Han, "Multiscale feature extraction of finger-vein patterns based on curvelets and local interconnection structure neural network," in *18th International Conference on Pattern Recognition (ICPR'06)*, vol. 4. IEEE, 2006, pp. 145–148.

[22] B. Huang, Y. Dai, R. Li, D. Tang, and W. Li, "Finger-vein authentication based on wide line detector and pattern normalization," in *2010 20th international conference on pattern recognition*. IEEE, 2010, pp. 1269–1272.

[23] H. Qin, M. A. El Yacoubi, J. Lin, and B. Liu, "An iterative deep neural network for hand-vein verification," *IEEE Access*, vol. 7, pp. 34 823–34 837, 2019.

[24] H. Jang, S. M. Plis, V. D. Calhoun, and J.-H. Lee, "Task-specific feature extraction and classification of fmri volumes using a deep neural network initialized with a deep belief network: Evaluation using sensorimotor tasks," *NeuroImage*, vol. 145, pp. 314–328, 2017.

[25] P. Liskowski and K. Krawiec, "Segmenting retinal blood vessels with deep neural networks," *IEEE transactions on medical imaging*, vol. 35, no. 11, pp. 2369–2380, 2016.

[26] S. Lin, T. Xu, and X. Yin, "Region of interest extraction for palmprint and palm vein recognition," in *2016 9th International Congress on Image and Signal Processing, BioMedical Engineering and Informatics (CISP-BMEI)*. IEEE, 2016, pp. 538–542.

[27] T.-C. Lee, R. L. Kashyap, and C.-N. Chu, "Building skeleton models via 3-d medial surface axis thinning algorithms," *CVGIP: Graphical Models and Image Processing*, vol. 56, no. 6, pp. 462–478, 1994.